Time-Domain Optical Response of an Electrooptic Modulator Using FDTD

Mahmoud Munes Tomeh, Sebastien Goasguen, *Student Member, IEEE,* and Samir M. El-Ghazaly, *Fellow, IEEE*

***Abstract*—A time-domain analysis of an $LiNbO_3$ electrooptic modulator using the finite-difference time-domain (FDTD) technique is performed. This allows for the calculation of optical modulation and the time-domain optical response of an electrooptic modulator. The electromagnetic fields computed by FDTD are coupled to standard electrooptic relations that characterize electrooptic interactions inside the embedded Ti diffused $LiNbO_3$ optical waveguides. The electric field-dependent change in the index of refraction inside these optical waveguides and resulting minute phase shifts imparted to optical signals propagating along the device are determined in time, allowing for the simulation of optical intensity modulation. This novel approach to $LiNbO_3$ electrooptic modulators using a coupled FDTD technique allows for previously unattainable investigations into device operating bandwidth and data transmission speed.**

***Index Terms*—Coplanar waveguides, electrooptic effects, electrooptic modulation, FDTD methods, optical fiber communication, optoelectronic devices.**

I. Introduction

SINCE THE early 1990's, the demand for capacity on North American long-distance fiber-optic networks has more than doubled every 18 months [1]. This insatiable demand for bandwidth is expected to continue on to 2005 and is being driven mostly by nonvoice data applications such as the Internet, video conferencing, e-mail, and fax. Such a large demand for bandwidth can only be met with long-haul fiber-optic systems. First-generation systems were based on directly modulated distributed feedback (DFB) lasers and could achieve modulation rates of 2.5 Gb/s. Such systems, however, suffer from the need for stations every 40 km to compensate for transmission loss and dispersion. External modulation with lithium niobate ($LiNbO_3$) electrooptic modulators has proven to be a substantial improvement to these first-generation systems. With $LiNbO_3$ external modulation systems, optical amplifier stations may be as far as 120 km apart or more [1], making long-distance transmission much more economical. For high-speed digital applications, optical-fiber dispersion severely limits system performance. $LiNbO_3$ electrooptic technology can contribute significantly to minimizing the effect of optical dispersion in optical fibers.

Manuscript received April 3, 2001; revised August 24, 2001.

M. M. Tomeh is with the Micro Photonix Integration Corporation, Phoenix, AZ 85029 USA (e-mail: M_Tomeh@mpi-ioc.com).

S. Goasguen is with the Electrical and Computer Engineering Department, Purdue University, West Lafayette, IN 47907 USA (e-mail: sebgoa@purdue.edu).

S. M. El-Ghazaly is with the Telecommunications Research Center, Arizona State University, Tempe, AZ 85287 USA (e-mail: sme@asu.edu).

Publisher Item Identifier S 0018-9480(01)10468-0.

Recently, $LiNbO_3$ technology has quickly matured from a mere laboratory curiosity to a practical technology. While niche markets such as microwave instrumentation [2] do and will continue to exist, cable TV (CATV) and long-haul telecommunications have been the market forces that have coaxed this theoretical toy of the physicist out to the market place. Recent advances now enable low driving voltage, low bias-voltage drift rates, and even bias-free devices.

As the push to realize bandwidths far beyond 40 Gb/s continues, the unique microwave design challenges posed by this problem will be more difficult to overcome. While quasi-static methods until now have been sufficient perhaps to yield accurate results, in the future the need for powerful simulation tools that will be both accurate and capable of simulating device performance will become far more urgent. Finite-difference time-domain (FDTD) techniques can be expected to play a very crucial role in future numerical developments in this field. FDTD in-time calculation of electric fields coupled with the electrooptic effect can provide for full simulation of a device time-domain optical response.

Published numerical work on the $LiNbO_3$ electrooptic modulator has concentrated on using static methods to optimize device geometry to meet various design constraints. Work has been done using finite elements method to find optimum electrode thickness and wall angle to achieve a good traveling wave—optical wave velocity match [3]. Other work has included more exotic techniques like the modified-step-segment method (MSSM) to analyze the optical waveguide region of this device [4]. No previous work, however, has proposed an intuitive approach to simulate complete device performance.

A radically new approach that utilizes a fully dynamic physical simulation of this device is proposed. The power of this approach is that it provides a complete simulation tool capable of being used to optimize device geometry to meet certain microwave design specifications as well as to optimize device optical performance by simulating the physical electrooptic interaction.

In this paper, we present many of the challenges and design strategies used to optimize device performance. We also present how the calculation of the time-domain optical response of electrooptic modulators is possible using FDTD. Section II will review the device structure and give a brief overview of the physical principles of device performance. Section III will discuss the main design constraints and the popular strategies employed to meet design objectives. Section IV will describe how FDTD can be used to compute the time-domain response of an electrooptic modulator. In Section V, some results derived from implementing the methods discussed in Section IV will be presented and discussed.

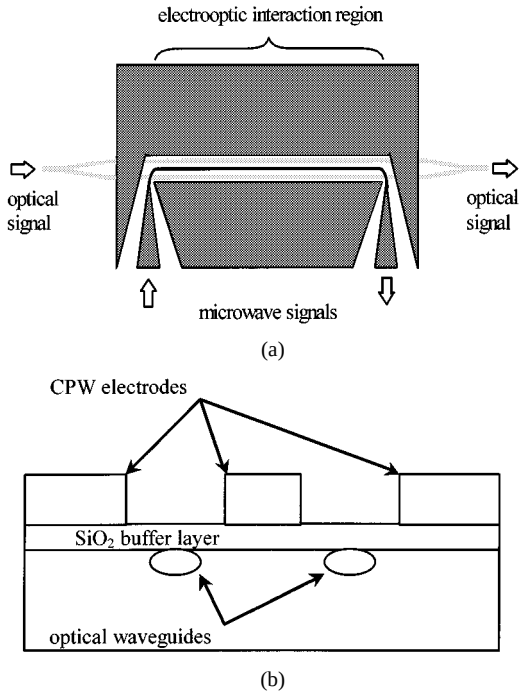

Fig. 1. Schematics showing: (a) the top view and (b) a cross-sectional view of a basic x-cut electrooptic modulator. The interaction region is essentially a CPW structure with optical waveguides in the electrooptically active $LiNbO_3$ substrate. Electric fields propagating along CPW structure change the phase of light traveling in each optical waveguide, which, upon interference, yields optical intensity modulation.

II. Electrooptic Modulator Device Structure

Briefly, this electrooptic modulator is a coplanar waveguide (CPW) structure with an anisotropic $LiNbO_3$ substrate that exhibits a Pockels electrooptic effect [5]. Electric fields applied to this substrate cause a change in its index of refraction that is proportional to the applied electric field. Inside this substrate are Ti diffused optical waveguides supporting optical signal propagation. This waveguide is split and comes in the close vicinity of a CPW structure to allow for electrooptic interaction. Electric signals traveling along the CPW structure induce electric fields in the substrate that change the phase of light traveling in the two embedded optical waveguides. After some interaction region, the optical waveguides combine, allowing the optical signals to interfere. Upon interference, the induced changes in phase translate into intensity modulation. For the modulation to be optimal (i.e., to maximize bandwidth), the velocity of electric signals traveling along the CPW structure and the optical signals traveling inside the embedded optical waveguides must be matched [6]. A basic sketch of device geometry is given in Fig. 1(a) and (b).

The relationship between the electric field and the change of index of refraction induced in $LiNbO_3$ is described by the following equations:

$$\begin{aligned}\Delta n_1 &= -\alpha n^3(r_{22}E_2 + r_{13}E_3)\\ \Delta n_2 &= -\alpha n^3(r_{22}E_2 + r_{13}E_3)\\ \Delta n_3 &= -\alpha n^3 r_{33}E_3\end{aligned} \tag{1}$$

where α, r_{22}, r_{13}, and r_{33} are constants, Δn_i is the change in index of refraction for optical fields polarized in the crystallographic i axis, and n is either the ordinary or extraordinary index of refraction [5]. Since r_{33} is the largest of the electrooptic coefficients, designs tend to try to maximize the electric field along the crystallographic z axis. Two main designs have been popular, x-cut and z-cut designs. An x-cut design typically places the optical waveguides symmetrically in the gaps of a CPW so that light traveling in the two waveguides will experience equal but opposite phase shifts. In the z-cut design, the waveguides are placed one underneath the central conductor, and another underneath one of the ground planes. Light traveling in these two waveguides will experience opposite but unequal phase shifts resulting in chirp. Negative chirp modulators help to minimize system degradation due to fiber dispersion. Fig. 2(a) and (b) depicts x- and z-cut modulator cross sections. These figures show the relative placement of optical waveguides with respect to CPW electrodes.

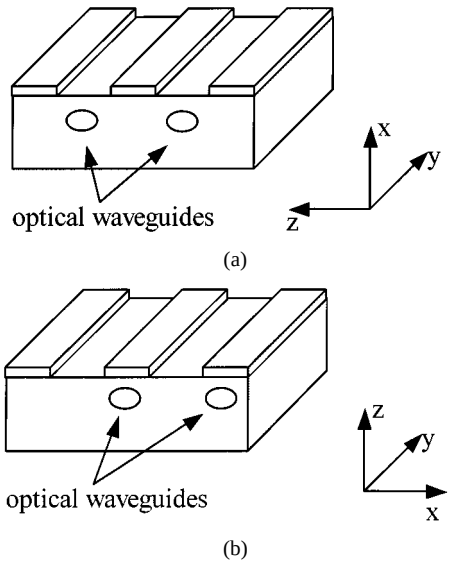

Fig. 2. (a) x-cut design attempts to harvest the electric field along the crystallographic z axis by placing optical waveguides in the centers of the gaps of the CPW structure. The two optical waveguides will experience equal and opposite electric fields. (b) z-cut design attempts to harvest the electric field along the crystallographic z axis by placing optical waveguides underneath the electrodes. The two optical waveguides will experience opposite, but unequal electric fields, which result in chirp.

III. Electrooptic Modulator Design

The primary design considerations for these devices are: 1) electric signal—optical signal phase velocity match; 2) low microwave losses; 3) 50-Ω CPW configuration; and 4) low driving voltage V_π (the voltage that must be applied to the RF electrodes which results in a total of π phase shift between the two legs of the electrooptic modulator resulting in zero intensity output). It is extremely difficult to simultaneously satisfy all four design goals, and hence tradeoffs become necessary.

The high value of the $LiNbO_3$ RF dielectric constants ($\varepsilon_r = 44, 28$) relative to the optical dielectric constants ($\varepsilon_r = 4.6, 4.9$) makes achieving electric signal—optical signal velocity match highly challenging. Invoking the static approximation to find the effective dielectric constant for microwaves propagating along CPW structure [2]

$$\varepsilon_{\text{eff}} = \frac{\sqrt{\varepsilon_x \varepsilon_y} + 1}{2} \tag{2}$$

yields a value of 18, more than three times the desired optical dielectric constant. In terms of phase velocity, this means that the CPW geometry must be designed to increase the phase velocity by a factor of two. Additionally, electrodes on $LiNbO_3$ substrate with no interlayered oxide buffer layer may have characteristic impedance values as low as 25 Ω or lower. Both velocity and impedance characteristics may be significantly improved utilizing low dielectric constant buffer layer between electrodes and $LiNbO_3$ substrate. Employing very thick electrodes [6] can also significantly speed up the microwave signal phase velocity. Other proposed strategies include utilizing a ridged waveguide structure [7] and buffer layer undercut beneath the electrode structures or electrode wall angle [3].

For typical devices, the gap and central conductor widths may be of the order of tens of micrometers. Since device geometry is on such a small scale, control of the phase velocity of waves traveling on these CPW structures by employing electrodes on the order of tens of micrometers or adding low dielectric constant buffer layers between electrodes and $LiNbO_3$ substrate of order one micrometer is possible. Thick electrodes, however, can severely compromise the characteristic impedance of the electrode, while thick buffers reduce the amount of electric field available in the optical waveguides to achieve phase shift. Finding a CPW configuration that allows for both a velocity-matched microwave signal and a 50-Ω electrode impedance is therefore difficult. Practical designs that match phase velocity have been reported with impedances as high as 40 Ω [8].

Many of these proposed strategies can help to significantly improve the design of electrooptic modulators. Fig. 3(a) and (b) suggests that SiO_2 buffer layers as thick as 1.2 μm can improve the impedance of the electrode structure and increase the phase velocity of the electric signals. However, even this buffer thickness has not resulted in a full phase velocity match.

Buffer layer undercuts can also help to increase the phase velocity as well as characteristic impedance. Fig. 4(a) suggests that a 50-Ω electrode is in fact achievable using a thick buffer layer in conjunction with a buffer layer undercut. Moreover, Fig. 4(b) shows that these configurations can in fact be phase velocity matched. Thick buffer layers and buffer undercuts, however, tend to reduce the electric field in the $LiNbO_3$ substrate available for electrooptic interaction, and hence such designs suffer from high V_π. This consideration tends to limit the usefulness of the thick buffer layer/buffer layer undercut strategies, and tradeoffs become necessary.

These data also demonstrate the need for full-wave analysis when operation frequencies approach or exceed 50 GHz since frequency dependence becomes important at these frequencies. The static techniques used so far to analyze these devices will suffer from inaccuracy at higher frequencies.

IV. Time-Domain Analysis of an Electrooptic Modulator

The flexibility and power of the FDTD method make it ideal for the unique numerical challenges posed by this problem, which include anisotropy and nonlinearity. Simulating the full optical response of the device is simply not possible using the static techniques applied so far to this problem.

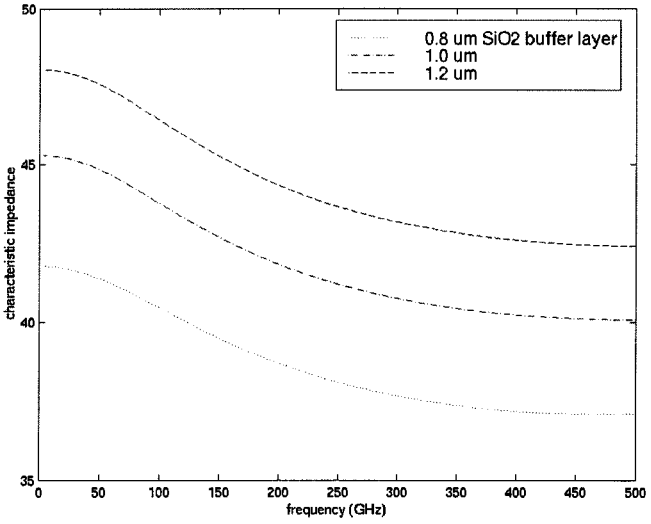

(a)

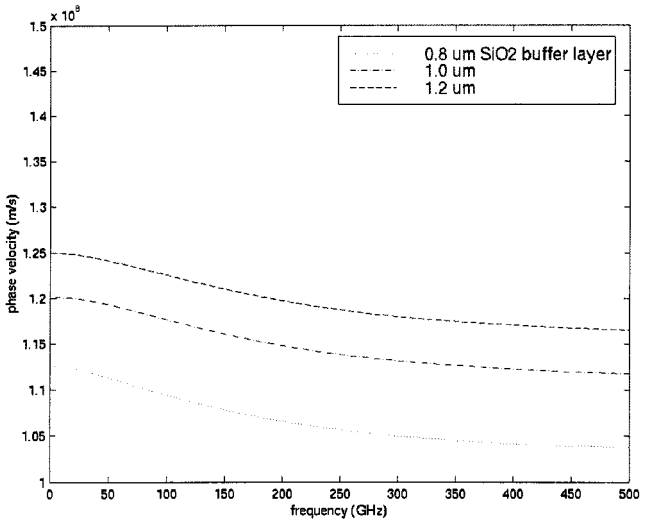

(b)

Fig. 3. (a) FDTD calculation of characteristic impedance as a function of frequency for several SiO_2 buffer layer thicknesses for a CPW structure with a 10-μm central conductor, a 10-μm gap width, and a 4-μm electrode thickness. (b) FDTD calculation of phase velocity as a function of frequency for several SiO_2 buffer layer thicknesses for a CPW structure with a 10-μm central conductor, a 10-μm gap width, and a 4-μm electrode thickness.

The power of FDTD lies in its full calculation of electric and magnetic fields. This is exploited by launching an electric Gaussian pulse along the CPW part of this device. The FDTD scheme calculates at each time step the electric field everywhere inside the device, including inside the embedded Ti diffused $LiNbO_3$ optical waveguide regions. This electric field information can then be coupled to the linear electrooptic effect using the electrooptic relations (1). These equations make it possible to compute the phase shift imparted to a light signal traveling in the vicinity of an electric signal in time. By adding the amplitudes of two optical signals a Mach–Zehnder interferometer is simulated resulting in device optical response.

Designs are currently typically based on simplified equations such as [8]

$$\Delta n = \frac{-n^3}{2} r \frac{V}{d} \Gamma \tag{3}$$

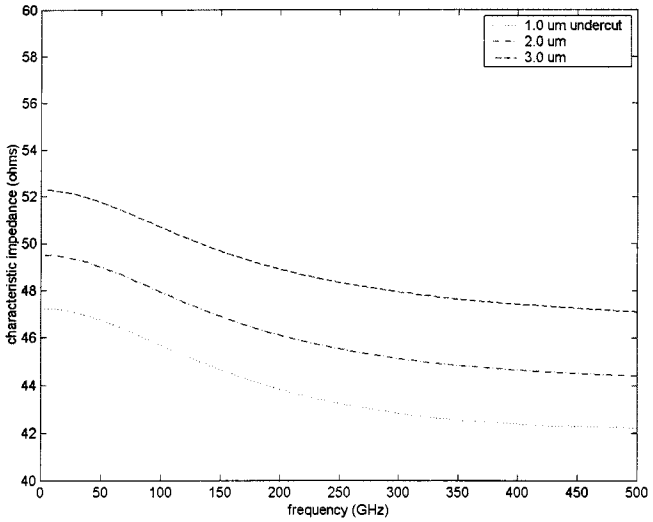

(a)

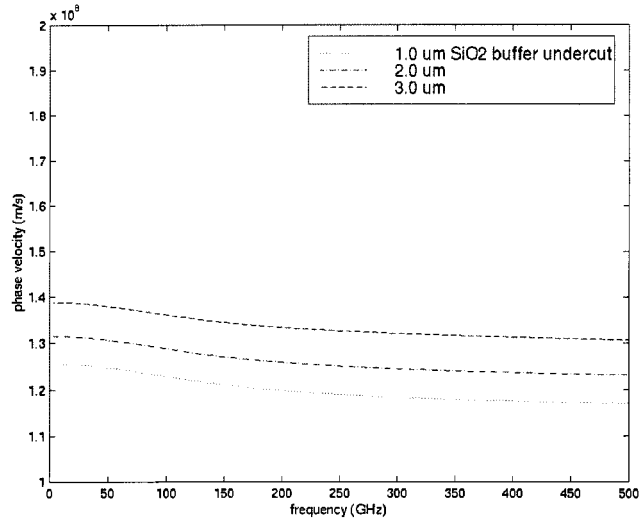

(b)

Fig. 4. (a) FDTD calculation of characteristic impedance as a function of frequency for several SiO_2 buffer layer undercuts for a CPW structure with a 10-μm central conductor, a 10-μm gap width, and a 4-μm electrode thickness. (b) FDTD calculation of phase velocity as a function of frequency for several SiO_2 buffer layer undercuts for a CPW structure with a 10-μm central conductor, a 10-μm gap width, and a 4-μm electrode thickness.

where r is the appropriate electrooptic coefficient, V/d is an ideal approximation to the electric field in between the CPW central conductor and the ground plane, and Γ is an empirically determined ratio used to improve the result since the V/d electric field approximation is crude. This equation is usually manipulated with the following equation that relates the phase shift imparted to an optical signal that has traveled over a length L with a change in index Δn:

$$\Delta\phi = \frac{2\pi}{\lambda_{\text{optical}}}\,\Delta nL. \tag{4}$$

These equations are typically used to calculate dc V_π and to find the appropriate interaction length, given a specific driving voltage. A clear improvement would be to replace the $\Gamma V/d$ with an accurate value for the electric field.

The FDTD calculation of the E-field throughout the device represents a profound improvement to the V/d approximation represented in (3). Since FDTD is a time-domain technique, the electrooptic modulator response may be calculated in time. This is accomplished by coupling these FDTD calculated electric field data with the physical electrooptic effect in time. From (3) and (4), one may derive an expression that describes the minute changes in phase induced in light signals interacting with electric fields at each time step of an FDTD scheme for optical signals traveling with a velocity $v_{\text{ph}}^{\text{optical}}$ $(= c/n_{\text{optical}})$. This can be done by replacing the length L in (4) with $v_{\text{ph}}^{\text{optical}}\Delta t$. This results in the following expression for the minute changes in phase imparted to optical signals at each FDTD time step Δt:

$$\delta_{\text{phase}} = -\frac{n^3\pi}{\lambda_{\text{optical}}}\,r_{33}v_{\text{ph}}^{\text{optical}}\Delta tE. \tag{5}$$

Since the spatial resolution (in the direction of both optical and electrical signal propagation) of the E-field data calculated using FDTD is not high enough for optical wave modeling, a standard interpolation scheme is used to generate a high-resolution electric field. Equation (5) is then used to find the minute changes in phase imparted to the optical signal at all points along the direction of propagation in the optical waveguides at each time step. These δ_{phase} data are then added to the overall phase of a sinusoidal wave used to model the optical signal.

An optical signal propagating in an embedded optical waveguide interacting with electric fields is represented as

$$\sin(\omega t - \beta z - \delta_{\text{phase1}}) \tag{6}$$

where ω and β are chosen appropriately for optical signals. Another optical waveguide carries an optical signal that is affected by the electric field in its vicinity. This optical signal is represented as

$$\sin(\omega t - \beta z - \delta_{\text{phase2}}). \tag{7}$$

The microwave electric field is given some distance to propagate and interact with the optical signal, representing the interaction region of the physical device. At each time step, to represent the motion of light through the wave guides, the $\delta_{phase}(z, t)$s will have to be shifted by a distance equal to the distance traveled by light in Δt. At each time step, the two sine waves represent the optical field along the complete length of the optical waveguide. To compute the optical response of the device, these two sine waves can be added at the end of the interaction region and be optical intensity computed. The FDTD simulation data to be presented represent an interaction length of the order of 2 mm. While realistic devices may have an interaction length one order of magnitude larger, such computations would be unreasonably long. As the computational speed of computers continues to increase, FDTD simulations may well be able to simulate practical devices of interaction lengths of the order of tens of millimeters in the near future.

V. Time-Domain Device Optical Response to a Gaussian Pulse

The ideas expressed in Section IV can be implemented in FDTD to yield a full time-domain optical response of electrooptic modulators to various electric signals. Here, the time-domain optical response to a Gaussian pulse is presented. The

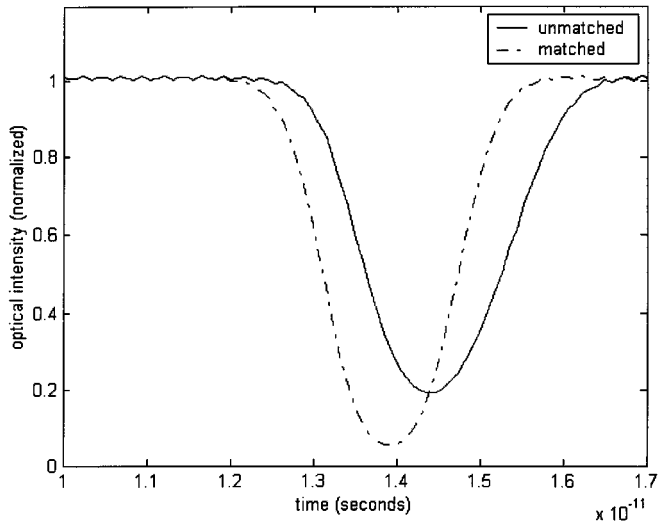

Fig. 5. Electrooptic modulator time-domain optical responses to a Gaussian electric pulse for two electrode designs representing an electrooptic phase velocity match and mismatch for the same interaction length (1.7 mm).

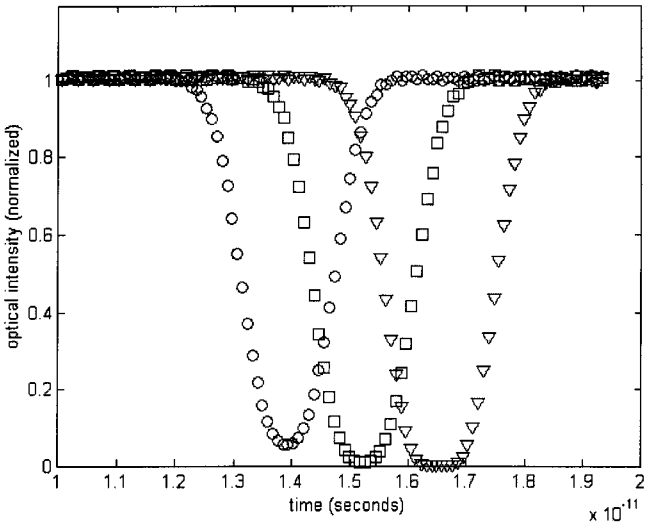

Fig. 6. Electrooptic modulator time-domain optical response to a Gaussian electric pulse for an electrode design representing an electrooptic phase velocity match for different electrooptic interaction lengths (circle: 1.7 mm, square: 1.9 mm, triangle: 2.1 mm).

FDTD simulation was of a $71 \times 151 \times 301$ cell structure, with 301 cells for the z axis (direction of propagation of electrical and optical signals). The cell size was 1 μm $\times$ 1 μm $\times$ 10 μm. The boundary conditions applied to the x and y faces of the computational domain were Mur boundary conditions, while in the direction of propagation, the boundary was set as a perfect electric conductor. This is justified since this boundary was significantly far away that the reflected wave is easily separated from the incoming wave. This was necessary since it is not clear how to implement a perfectly matched layer (PML) with an anistropic substrate in the computational domain and $LiNbO_3$ is anisotropic. This simulation was run on PCs with 933-MHz processors with a run time on the order of 24 h. Two CPW structures have been simulated with different phase velocities resulting from different electrode thicknesses. The CPW structure with a thick electrode has a phase velocity that is more closely matched than the structure with a thin electrode. Comparing the response of these two CPW structures will demonstrate how phase velocity mismatch can affect the performance of electrooptic modulators. The matched condition for these calculations is taken to be $n_{\text{optical}} = 2$. The constants in (5) are lumped into one constant, for purposes of demonstration, with the value of 0.000125. One waveguide is taken to be in the center of one of the gaps and is assumed to be affected by the electric field of only one line parallel to this gap. The other optical waveguide is taken to be unaffected by any electric field.

Fig. 5 shows a direct comparison of two time-domain electrooptic responses for the matched and mismatched cases. Fig. 5 shows a wider unmatched optical response, which is intuitively understood since the peak electric signal applies phase shift over a larger region of the optical signal than in the matched case. Similarly, such an unmatched signal will result in a higher V_π for a given electrooptic interaction length. Fig. 5 also numerically demonstrates how important electrooptic phase velocity match is to bandwidth of electrooptic modulators, especially for digital applications where the wider time domain response can be clearly seen to limit the time-domain proximity of two bits for data transmission.

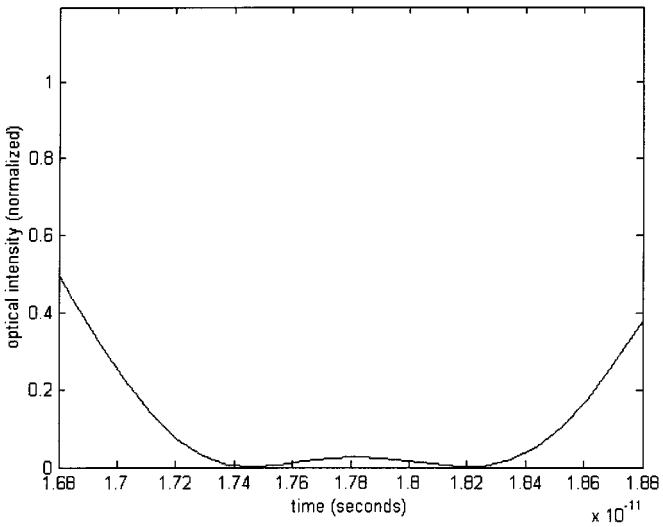

Fig. 7. Electrooptic modulator time-domain optical response to a Gaussian electric pulse for an electrode design representing an electrooptic phase velocity match for a long electrooptic interaction length (2.1 mm) that results in phase reversal.

Given a defined driving voltage and desired V_π, the interaction length of electrooptic modulators must be properly designed so as not to be too short so that the optical response is too shallow, nor too long so that the optical response will exhibit phase reversal. Fig. 6 shows the optical response to an electric Gaussian pulse for different lengths of electrooptic interaction regions for the matched case.

In Fig. 6, it is seen that the optical response is just beginning to exhibit phase reversal. If the interaction region is made just a bit longer, this matched electrooptic modulator will exhibit phase reversal for the given driving voltage. Such phase reversal is represented in Fig. 7.

Fig. 8 displays results for the unmatched case, for which the pulses are much wider, and V_π has significantly increased.

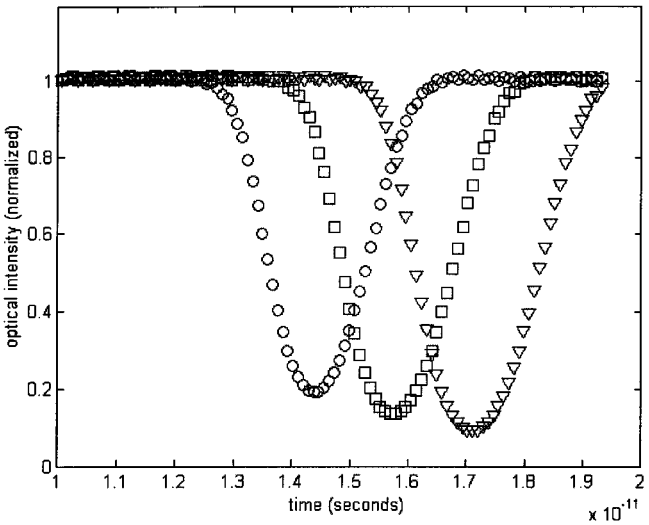

Fig. 8. Electrooptic modulator time-domain optical response to a Gaussian electric pulse for an electrode design representing an electrooptic phase velocity mismatch for different electrooptic interaction lengths (circle: 1.7 mm; square: 1.9 mm; triangle: 2.1 mm).

VI. Conclusion

FDTD provides for a fully intuitive approach to the simulation of electrooptic modulator optical response. While it is clear that FDTD can be used to characterize the CPW structure, it can also be a powerful tool in understanding the effects of device geometry on optical response. Using an FDTD solution of the E-field in time coupled to electrooptic interactions, a fully physical simulation of electrooptic modulators is possible. Coupled FDTD calculations presented here have numerically demonstrated the dependence of electrooptic modulator performance on velocity matching. Comparisons between the matched and unmatched cases have shown the effect of phase velocity matching on bandwidth, driving voltage, and interaction length. Precise modeling of electrooptic modulators using coupled FDTD can be expected to contribute significantly to improved device performance in the future.

Acknowledgment

The authors wish to express gratitude for the generous support and fruitful collaboration of Micro Photonix Integration Corporation, Phoenix, AZ.

References

[1] E. J. Murphy, "Commercialization of lithium niobate modulators," in *Integrated Optical Circuits and Components: Design and Applications*, E. J. Murphy, Ed. New York: Marcel Dekker, Aug. 1999.

[2] R. L. Jungerman, C. Johnsen, D. J. McQuate, K. Salomaa, M. P. Zurakowski, R. C. Bray, G. Conrad, D. Cropper, and P. Hernday, "High-speed optical modulator for application in instrumentation," *J. Lightwave Technol.*, vol. 8, pp. 1363–1370, Sept. 1990.

[3] G. K. Gopalakrishnan, W. K. Burns, R. W. McElhanon, C. H. Bulmer, and A. S. Greenblatt, "Performance and modeling of broadband $LiNbO_3$ travelling wave optical intensity modulators," *J. Lightwave Technol.*, vol. 12, pp. 1807–1819, Oct. 1994.

[4] K. Kawano, "High-speed shielded velocity-matched $Ti:LiNbO_3$ optical modulator," *IEEE J. Quantum Electron.*, vol. 29, pp. 2466–2475, Sept. 1993.

[5] G. K. Gopalakrishnan, C. H. Bulmer, W. K. Burns, R. W. McElhanon, and A. S. Greenblatt, "40 GHz low half-wave voltage $Ti:LiNbO_3$ intensity modulator," *Electron. Lett.*, vol. 28, no. 9, pp. 826–827, 1992.

[6] K. Noguchi, L. Mitomi, K. Kawano, and M. Yanagibashi, "Highly efficient 40-GHz bandwidth $Ti:LiNbO_3$ optical modulator employing ridge structure," *IEEE Photon. Technol. Lett.*, vol. 5, pp. 52–54, Jan. 1993.

[7] E. L. Wooten, K. M. Kissa, A. Yi-Yan, E. J. Murphy, D. A. Lafaw, P. F. Hallemeier, D. Maack, D. V. Attanasio, D. J. Fritz, G. J. McBrien, and D. E. Bossi, "A review of lithium niobate modulators for fiber-optic communications systems," *IEEE J. Quantum Electron.*, vol. 36, pp. 69–82, Jan. 2000.

[8] S. K. Korotky and R. C. Alferness, "$Ti:LibNO_3$ integrated optic technology," in *Integrated Optical Circuits and Components: Design and Applications*, L. D. Hutcheson, Ed. New York: Marcel Dekker, Aug. 1987.

Mahmoud Munes Tomeh received the B.A. degree in physics from the University of California at Berkeley, in 1995, and is currently working toward the M.S. degree in electrical engineering at Arizona State University, Tempe.

In 1999, he joined the Microwave Circuits Laboratory, Arizona State University, as a Research Assistant.

Sebastien Goasguen (S'01) was born on March 22, 1974, in Rennes, France. He received the B.S. degree in electrical engineering from the Polytechnic Institute of Toulouse, Toulouse, France, in 1997, the M.S. degree (with honors) in electronics research from the King's College, London, U.K., in 1998, and the Ph.D. degree from Arizona State University, Tempe, in 2001.

His area of research is large and ranges from linearization techniques and monolithic-microwave integrated-circuit (MMIC) design to numerical techniques and semiconductor modeling. In September 2001, he began a full-time post-doctoral position with the Electrical and Computer Engineering Department, Purdue University, West Lafayette, IN, where he is involved in nanotechnology and molecular electronics.

Samir M. El-Ghazaly (S'84–M'86–SM'91–F'01) received the Ph.D. degree in electrical engineering from the University of Texas at Austin, in 1988.

In August 1988, he joined the Arizona State University, Tempe, where he is currently a Professor in the Department of Electrical Engineering. He has visited and worked at several universities and research centers, including Cairo University, Cairo, Egypt, the Centre Hyperfrequences et Semiconducteurs, Université de Lille I, Lille, France, the University of Ottawa, Ottawa, ON, Canada, the University of Texas at Austin, the NASA Jet Propulsion Laboratory, Pasadena, CA, CST–Motorola Inc., Tempe, AZ, *iemn*, Université de Lille, Lille, France, and the Swiss Federal Research Institute (ETH), Zurich, Switzerland. His research interests include RF and microwave circuits and components, microwave and millimeter-wave semiconductor devices, semiconductor device simulations, ultrashort pulse propagation, microwave-optical interactions, linear and nonlinear modeling of superconductor microwave lines, wave–device interactions, electromagnetics, and numerical techniques applied to monolithic microwave integrated circuits.

Dr. El-Ghazaly is a Fellow of IEEE. He is an elected member of Commissions A and D of URSI, and a member of Tau Beta Pi, Sigma Xi, and Eta Kappa Nu. He was the secretary and vice-chairman and is currently the chairman of Commission A of the U.S. National Committee of URSI. He is a member of the Technical Program Committee for the IEEE IMS since 1991, and is on the Editorial Board of the IEEE TRANSACTIONS ON MICROWAVE THEORY AND TECHNIQUES. He was the chairman of the IEEE Waves and Devices Group, Phoenix Section. He was the chapter funding coordinator and chairman of the Chapter Activities Committee of the IEEE MTT-S. He is an elected member of the AdCom of the IEEE MTT-S. He is the editor-in-chief for the IEEE MICROWAVE AND WIRELESS COMPONENTS LETTERS. He was the general chairman of the IEEE MTT-S 2001 IMS, held in Phoenix, AZ, May 2001.